M. Stöhr, Z. Yin and W. Meier, Interaction between velocity fluctuations and equivalence ratio fluctuations during thermoacoustic oscillations in a partially premixed swirl combustor, Proceedings of the Combustion Institute 36 (2017) 3907–3915.

The original publication is available at www.elsevier.com

http://dx.doi.org/10.1016/j.proci.2016.06.084

Interaction between velocity fluctuations and equivalence ratio fluctuations during thermoacoustic oscillations in a partially premixed swirl combustor

M. Stöhr[a,*], Z. Yin[a], W. Meier[a]

[a]*German Aerospace Center (DLR), Institute of Combustion Technology, Pfaffenwaldring 38-40, 70569 Stuttgart, Germany*

Abstract

The combined effects of velocity fluctuations (VF) and equivalence ratio fluctuations (ERF) on thermoacoustic flame oscillations are studied experimentally in a gas turbine model combustor. The analysis is based on time-resolved simultaneous measurements of flow field, flame structure and fuel distribution using combined PIV, OH-PLIF and tracer-PLIF at a rate of 10 kHz. In order to separate the effects of VF and ERF, the combustor has been operated in two configurations: a technically (i.e. partially) premixed (TP) configuration where both ERF and VF occur, and a perfectly premixed (PP) configuration where only VF are present. A particular operating condition is selected where the VF are similar for both premixing modes. The corresponding fluctuations of heat release, by contrast, exhibit considerably different spatial patterns for the two modes. In particular, periodic widening and narrowing as well as extinction and re-ignition of the flame base, and a convective motion of the flame zone are observed in the TP flame but not in the PP case. An evaluation of periodic variations of flux rates and heat release shows that the feedback loop of the TP flame includes an additional convective delay of 50°. The time-resolved measurements reveal that this delay leads to a coincidence of fuel-lean unburned gas and high velocity that induces local flame extinction and narrowing of the flame base. When the equivalence ratio later increases, the flame base re-ignites and a widened zone of increased heat release forms that is convected downstream. For the PP case, by contrast, reaction at the flame base is stable and accordingly the flame responds earlier to VF compared to the TP case. The results show that interacting VF and ERF have a strong and complex impact on the thermoacoustic response of turbulent swirl flames, and this impact depends largely on their time-delay.

Keywords: Thermoacoustic instability, Turbulent swirl flames, Flow-chemistry interaction, Gas turbine combustion, High-speed laser diagnostics

1. Introduction

For modern, lean, low-emission gas turbine (GT) combustors, the prevalent susceptibility to thermoacoustic pressure pulsations [1] poses a major problem for the development of combustors with improved emissions and operational flexibility. The feedback loop of these thermoacoustic instabilities is determined by highly complex, multi-scale transient interactions of acoustics, turbulent flow, mixing and reaction [2], which are difficult to model even with expensive modern CFD tools. The design of improved combustors therefore requires further basic understanding of these interactions based on detailed experimental data.

For a closed feedback loop, it is necessary that the acoustic oscillations excite a varying heat release of the flame. It is widely established [3, 4, 5, 6] that this mainly takes place in two ways, namely through velocity fluctuations (VF) and equivalence ratio fluctuations (ERF) (other effects, such as entropy waves, are neglected in this work). VF lead to a varying flux of unburned gas into the flame zone, and subsequently to changes of, e.g., flame surface density, vorticity or strain rate [7]. ERF are caused by fluctuations of velocity or pressure at the point of fuel injection [8, 9, 10], which induce local inhomogeneities of fuel-air mixture propagating into the combustion chamber. This leads to a varying equivalence ratio of the unburned gas entering the flame zone, and hence variations of heating value, flame speed and flame surface density [11]. In GT burners with perfect premixing (PP), where fuel and air are mixed far upstream of the flame, only VF can be present. In order to avoid safety risks such as auto-ignition or flashback, however, most burners are operated in a partially premixed or technically premixed (TP) mode, where fuel is injected shortly upstream of the burner nozzle, and thus both ERF and VF occur.

A number of studies has shown that VF and ERF cannot be treated separately, but interact in various ways. Comparing results from PP and TP operation of a combustor, it was found that ERF, often depending on their convective time lag, can either enhance or dampen the flame response to VF [9, 7, 5, 6]. It was further observed that non-linear effects of the TP flame response, such as saturation at high amplitude, depend on the phase difference between VF and ERF [4]. Cosic et al. [6] concluded that an increase of VF enhances fuel-air mixing and thus causes saturation of the flame response. The phenomena reported in these works are the result of intricate interactions

*Corresponding author. Email: michael.stoehr@dlr.de

amongst flow field, mixing and flame propagation taking place on a wide range of spatial and temporal scales, which are not well understood to date. Elucidating these mechanisms requires time-resolved multi-parameter diagnostics that was not available in previous works.

The aim of this work is to study the mechanisms of transient interactions between VF and ERF in a GT-typical turbulent swirl flame, and relate them to the observed global flame oscillation. For this purpose, the work employs a combustor that can be operated both in PP [13, 14, 15] and TP [12, 15] mode. Flow field, flame structure and fuel distribution are measured simultaneously in a 2D domain using combined time-resolved stereo-PIV, OH-PLIF and tracer-PLIF. In order to separate the effects of VF and ERF, measurements are performed in both PP and TP mode at a specific condition where the respective VF are nearly equal. The respective patterns of heat release variation, on the other hand, exhibit pronounced differences between the two modes. These differences are then traced back to the transient combined effects of VF and ERF seen in the time-resolved measurements like, e.g., local flame extinction or changes of local flame speed. Furthermore, the combined measurements of velocity field and fuel distribution are used for a quantitative analysis of oscillating fluxes of unburned fuel and air and their role in the global feedback cycle.

2. Experimental setup

2.1. Combustor and operating condition

The schematics of the two versions of the gas turbine model combustor are shown in Fig. 1. The burner is derived from a design by Turbomeca and has been investigated experimentally (e.g., [12, 13, 14, 15]) and numerically (e.g., [16, 17, 18]) within and after the PRECCINSTA EU project. It is composed of a cylindrical plenum (d=78 mm), a swirl generator with 12 radial vanes, a converging nozzle (d=27.85 mm) with a central conical bluff body, and a combustion chamber. The chamber has a square cross-section of 85×85 mm^2 and a height of 114 mm, and an exit with a conical part followed by an exhaust duct (d=40 mm). Optical access to the chamber is provided by side walls made of quartz glass. A sonic nozzle is installed in the supply line to the plenum in order to uncouple the combustor acoustics from the gas supply.

For the PP version, fuel and air are fully mixed upstream of the sonic nozzle where no pressure fluctuations from the burner can be present. In the TP version, fuel is injected into the air flow through small holes (d=1 mm) in a jet-in-crossflow configuration within the radial swirler. The measurements are performed at atmospheric pressure and with methane as the fuel.

No general dependence of thermoacoustic amplitude on premixing mode was found, i.e., for some conditions the PP and for others the TP configuration has higher amplitude. For the present study, an operating condition with a thermal power of P_{th}=15 kW and an equivalence ratio of ϕ_{global}=0.8 was selected, where the amplitude is almost equal for both premixing modes as specified in Table 1. The respective VF are therefore expected to be similar for both modes, which allows for a good separation of the effects of ERF in the TP mode. For both modes the flame has a similar V-shaped form as shown in Fig. 1. Both flames do not exhibit a precessing vortex core (cf. Ref. [14]).

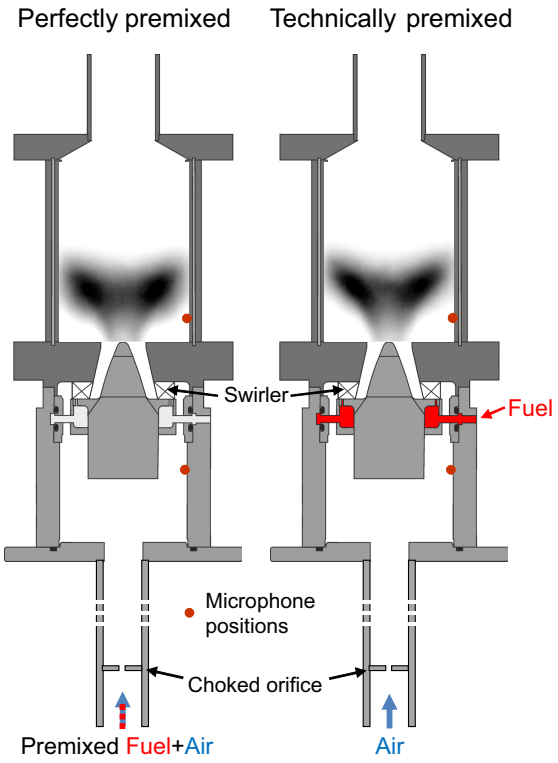

Figure 1: Geometry of gas turbine model combustor for PP (left) and TP (right) configuration. OH-CL images of flame shape are shown for P_{th}=15 kW and ϕ=0.8.

	Amplitude L [dB]	Frequency f [Hz]	Period $T=\frac{1}{f}$ [ms]
PP	141.5	296	3.4
TP	141.1	264	3.8
TP with 15% acetone	140.8	255	3.9

Table 1: Amplitudes and frequencies of thermoacoustic oscillation.

For the measurement of fuel distribution using acetone-PLIF as described below, 15 Vol% acetone was added to the methane, and the flow rates of air and methane were adjusted such that P_{th} and ϕ_{global} remain constant. At this acetone content, both a good LIF signal was obtained, and the influence of acetone on the flame was low (see Table 1).

2.2. Measuring techniques

The time-resolved measurements were made using an enhanced version of the simultaneous PIV, OH-PLIF and acetone-PLIF system described in Ref. [20]. The following description provides the most important specifications and the extensions implemented in this work.

The PIV system employs a dual-cavity Nd:YAG laser (Edgewave IS-6IIDE, 2.6 mJ/pulse at 532 nm) and has now been extended to a stereo-PIV setup using 2 CMOS cameras (LaVision HSS 8). OH-PLIF and acetone-PLIF were both excited at 283.2 nm by the same dye laser (Sirah Credo, 80 μJ/pulse at 283.2 nm) pumped with a Nd:YAG laser (Edgewave IS-8IIE, 4 mJ/pulse at 523 nm). The beams of the two laser systems were expanded into two coplanar vertical light sheets across the central section of the combustion chamber. About 4% of the UV light sheet was deflected into a cuvette filled with a fluorescent liquid for sheet profile imaging. For PIV the air flow was seeded with TiO_2 particles with a nominal diameter of 1 mm. For the present conditions their Stokes number is <0.02 (cf. Ref. [14]), and therefore they accurately follow the unsteady flow.

The OH-PLIF emission was recorded using an intensified CMOS camera (LaVision HSS 5 with HS-IRO) equipped with a Cerco UV lens (f=45 mm, f/1.8) and a bandpass filter (300-325 nm). The acetone-PLIF emission, which is spectrally well separated from that of OH, was recorded using an intensified CMOS camera (LaVision HSS 6 with HS-IRO) equipped with a Canon lens (f=85 mm, f/1.2). Single-shot images of the UV laser sheet profile in the dye cuvette were recorded using an intensified CMOS camera (LaVision HSS 5 with HS-IRO) equipped with a Nikon lens (f=50 mm, set to f/4).

All lasers and cameras were running with a repetition rate of 10 kHz, and the sustained recording time was 0.8 s corresponding to 8000 single measurements. The measurement domains were restricted to heights of 30 mm (PIV), 40 mm (OH-PLIF) and 21 mm (acetone) above the nozzle. The PIV images were processed using a cross-correlation algorithm (LaVision DaVis 8.2) with a final interrogation window size of 16 $\times$ 16 pixel, resulting in velocity fields with an in-plane spatial resolution of 1.3 $\times$ 1.3 mm^2. Based on the $\pm$0.1 pixel uncertainty of the cross-correlation peak-finding algorithm, the random uncertainty of the PIV measurements is estimated as $\pm$0.6 m/s. The single-shot inhomogeneities and energy fluctuations of the PLIF laser sheet were corrected using the simultaneously recorded dye cuvette sheet profiles. The acetone-PLIF images were further processed as described in Sect. 3.

Additional stereo-PIV and OH chemiluminescence (CL) measurements with a repetition rate of 5 Hz covering the full cross-section of the combustion chamber were performed using the setup described in Ref. [14], where also uncertainties are discussed.

Pressure fluctuations were measured by two microphones (Brüel & Kjaer), one attached to a post in the corner of the combustion chamber at y=16 mm, and the other at half height of the plenum wall. In the plenum the microphone is flush mounted to the wall, whereas at the chamber an acoustic probe is used where the microphone is located $\approx$15 cm away from the corner post in order to protect it from heat. The acoustic effects of the probe are determined by a calibration, and the measured data is corrected for these effects. Using a multichannel DAQ, the microphone signals and the laser trigger signal were continuously recorded during a series of measurements. This allows the determination of the phase-angle φ of the thermoacoustic oscillation for each individual measurement. The phase angle φ=0° is defined as the negative-to-positive transition of pressure in the plenum.

3. Estimation of volumetric flow rates

3.1. Calibration of tracer-PLIF signal and image processing

This section describes the estimation of the oscillating equivalence ratio and fluxes of unburned air and fuel into the combustion chamber, which are an integral part of the analysis of the thermoacoustic feedback loop in Sect. 4.2. The estimation is based on the previously specified simultaneous measurements of velocity field and acetone distribution, and its main processing steps are described below.

At first, a calibration was performed where fuel-air mixtures with defined equivalence ratios in the range $0.6<\phi<3$ were introduced into the chamber at a temperature of $T\approx25\,^{\circ}$C, and for each value of ϕ an average acetone-PLIF image was obtained. A highly linear relationship (R^2=0.998) between acetone-PLIF signal and equivalence ratio was obtained in this range of ϕ. This relation, however, is only valid for $T\approx25\,^{\circ}$C because the density and thus also the PLIF signal decreases when temperature rises. Since the following estimation evaluates equivalence ratios at y=2 mm, where the temperature of unburned gas is about T=50°C according to Raman measurements [12], the calibration factor has been corrected by the corresponding density ratio (effects of varying fluorescence yield are neglibible in this temperature range for excitation at 283 nm [19]). Further downstream, the temperature of the unburned gas may change significantly, and since no planar temperature measurements are available, no quantitative fields of ϕ can be derived from the 2D acetone-PLIF distributions later in Figs. 3 and 5.

The equivalence ratio ϕ and the volumetric fluxes of unburned air and fuel into the chamber, determined at the plane y=2 mm, are then estimated for each simultaneous PIV and acetone-PLIF measurement. Firstly the radial range of unburned gas near the nozzle exit is determined from the PIV particle images as shown exemplarily in Fig. 2. The locating of unburned gas is based on the fact that its (particle) density is about 6.5 times higher than that of burned gas due to thermal expansion. The grainy particle image (Fig. 2a) is smoothed using a sliding median filter (Fig. 2b), and the radial range of unburned gas at y=2 mm is determined using an appropriate threshold value (green lines). In Fig. 2c, this range is marked in the corresponding simultaneous PIV, OH-PLIF and acetone-PLIF measurement.

The total volumetric flow rate of unburned air and fuel Q_{total} is then determined as

$$Q_{\mathrm{total}} = \int_{r_{\mathrm{u}}} v_y(r)\,\pi\,r\,dr, \tag{1}$$

and the volumetric flow rate of fuel Q_{fuel} as

$$Q_{\mathrm{fuel}} = \int_{r_{\mathrm{u}}} v_y(r)\,c(\phi(r))\,\pi\,r\,dr. \tag{2}$$

Here v_y denotes the axial velocity, c is the fuel concentration associated with the local value of ϕ, and r_{u} denotes the range of

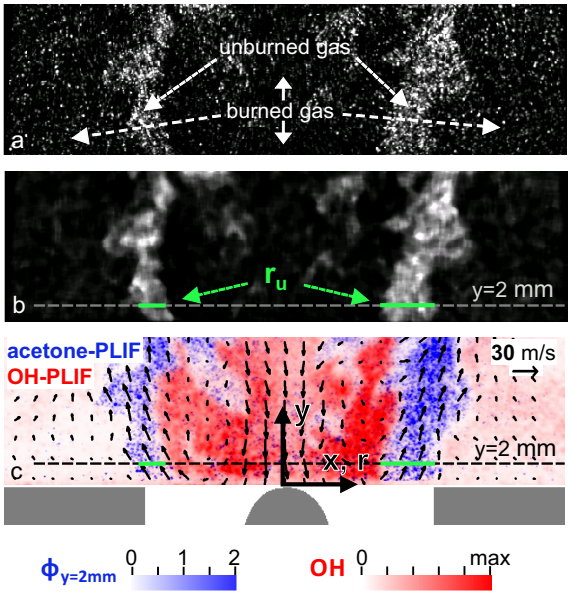

Figure 2: Estimation of Q_{total}, Q_{fuel} and ϕ_{u} using (a) original and (b) smoothed PIV particle image and (c) combined fields of velocity, OH and acetone.

unburned gas (green lines). Finally, the equivalence ratio of the unburned gas ϕ_{u} at y=2 mm is calculated as

$$\phi_{\text{u}} = \frac{1}{A_{\text{u}}} \int_{r_{\text{u}}} \phi(r)\, \pi\, r\, dr, \qquad (3)$$

with $A_{\text{u}} = \int_{r_{\text{u}}} \pi\, r\, dr$.

It is noted that values of Q_{total}, Q_{fuel} and ϕ_{u} based on a single planar measurement through a 3D flow do not provide valid estimates because the instantaneous flow is not axisymmetric. For the analyses in Sects. 4.2 and 3.2, however, only phase-averages, based on about 1000 single measurements per phase angle, or full averages based on 8000 measurements are considered. In this case, a sufficient sampling of circumferential fluctuations takes place, such that the values are considered as a valid representation of the, on (phase-)average, axisymmetric 3D flow.

3.2. Uncertainties and validation against average fluxes

The major sources of error for Q_{total}, Q_{fuel} and ϕ_{u} and their respective values of uncertainty were determined as follows. The most critical issue for all 3 quantities is the correct localization of the range of unburned gas, over which the integration in Eqs. (1)–(3) is performed. The localization is affected by the choice of the threshold value and pulse-to-pulse variations of the PIV laser sheet (which were not monitored), and causes an uncertainty of about 8% for Q_{total}, Q_{fuel} and ϕ_{u}. An additional uncertainty of Q_{fuel} and ϕ_{u} of about 6% originates from uncertainties of $\phi(r)$ and $c(r)$ due to PLIF laser beam absorption. In comparison, other errors from, e.g., velocity measurement or acetone-PLIF calibration, are relatively low and therefore neglected.

In Table 2, the average values of Q_{total}, Q_{fuel} and ϕ_{u}, based on a series of 8000 measurements in the TP flame, are compared to

	Preset value	Data analysis
$\overline{Q}_{\text{total}}$ [l/s]	6.5±0.1	7.0±0.6
$\overline{Q}_{\text{fuel}}$ [l/s]	0.43±0.005	0.46±0.05
$\overline{\phi}_{\text{u}}$	0.80±0.01	0.73±0.07

Table 2: Comparison of estimated averages of Q_{total}, Q_{fuel} and ϕ_{u} with preset values.

values corresponding to the preset flow rates of the combustor gas supply. The values agree within differences <10%, which conforms with the above analysis of uncertainties.

4. Comparison of PP and TP flame oscillations

4.1. Phase averages of velocity field and OH-CL

The thermoacoustic oscillations of the flames in PP and TP mode are compared in Fig. 3 using 8 phase-averages (φ=0°, 45°, ..., 315°) of velocity field, heat release and fuel distribution. The comparison of velocity fields shows that the variation of flow field is almost the same for both modes. This is expected since the variation is mainly caused by the acoustic particle velocity, and both flames have a similar acoustic frequency and amplitude (cf. Table 1). For both modes the phase-averages reveal a strong fluctuation of flow into the chamber with a minimum at φ≈45° and a maximum at φ≈225°.

The phase-averages of heat release are based on line-of-sight integrated OH-CL images that have been Abel-deconvoluted to obtain the associated 2D distributions in the center plane. In contrast to the velocity field, strong differences appear in the dynamics of heat release. For the PP flame, reaction takes place continuously in the inner shear layer, while the global intensity varies between its maximum at φ≈45° and the minimum at φ≈225°. For the TP flame, on the other hand, a strong convective displacememt of heat release takes place. After the global minimum at φ=270°, the reaction rate first increases at the flame root near the nozzle (φ=315°), and then the flame zone propagates downstream (φ=0° to 180°, marked with red lines). Furthermore, a pronounced narrowing (φ=225°) and widening (φ=45°) of the flame base is observed that is not seen in the PP case. At φ=180°, heat release at the flame base almost disappears, indicating that at least partially an extinction of reaction zone occurs. The transient interactions of flow, mixing and reaction that are causing these phenomena are discussed using time-resolved measurements in Sect. 5.

Since the velocity variations are nearly the same for both modes, the differences of heat release dynamics of the two modes can only originate from ERF that are solely present in TP mode. The phase-averaged acetone-PLIF distributions in Fig. 3 show that indeed, strong ERF occur in the TP flame between a minimum at φ=90° and a maximum at φ=270°. The role of these fluctuations in the thermoacoustic feedback loop is analyzed in the following subsection.

4.2. Periodic variations of flux rates, ϕ and heat release

The phase-averages in Fig. 3 indicate that the thermoacoustic feedback loop is an interplay of heat release fluctuations and

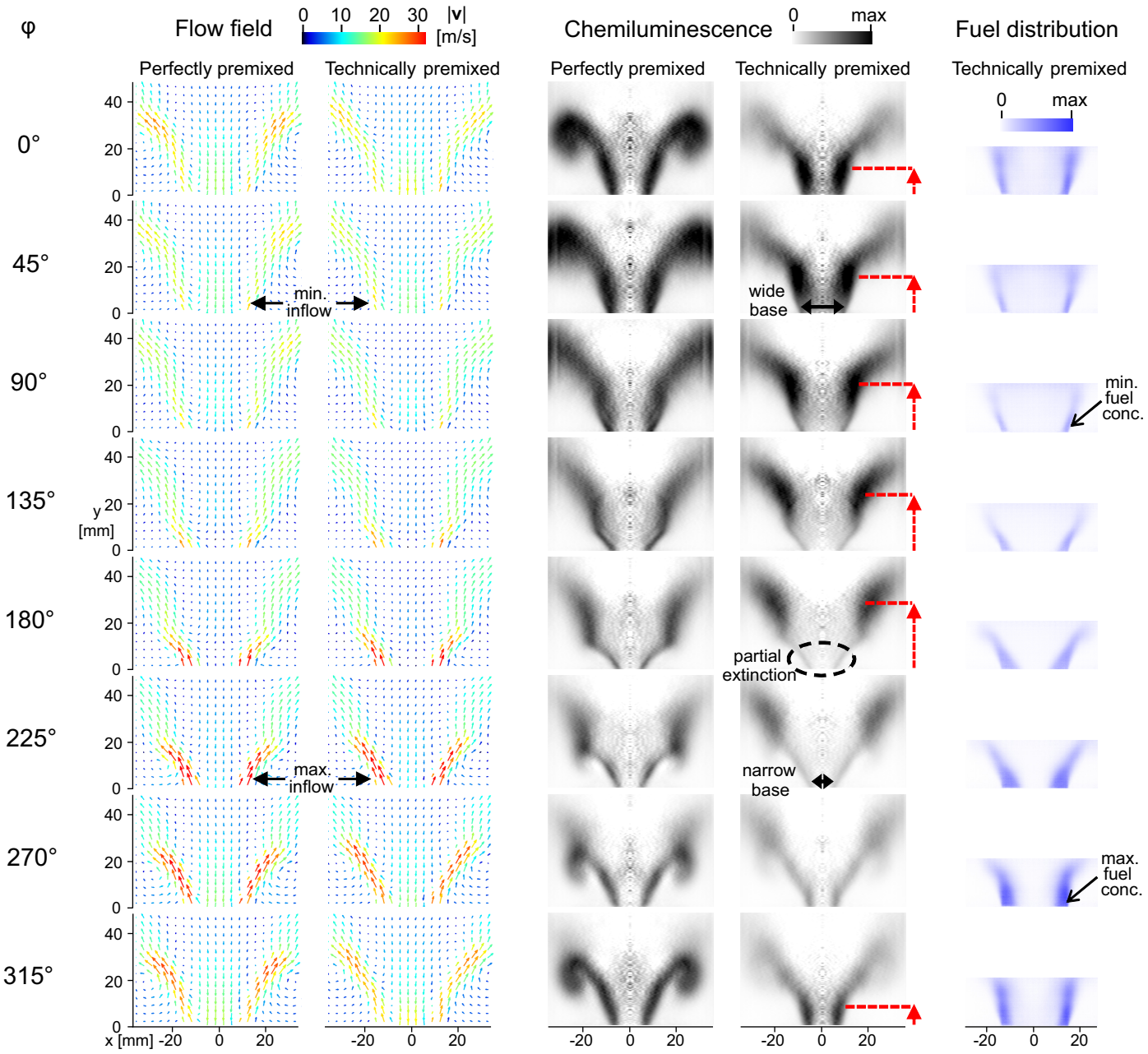

Figure 3: Phase averages of velocity field, abel-deconvoluted OH-CL and acetone-PLIF for the PP and TP flame.

varying fluxes of unburned fuel and air into the chamber. In order to work out the effect of ERF in this loop, the phase-averages of ϕ_u and the fluxes of unburned gas Q_{total} and fuel Q_{fuel} were estimated as described in Sect. 3. The results are plotted in Fig. 4 together with the variation of global heat release.

The variations of the flux of unburned gas Q_{total} are almost identical for both premixing modes with a common maximum at φ=200°, as expected from the similarity of velocity variations in Fig. 3. Notably, for the TP flame the equivalence ratio ϕ_u of the incoming flow reaches its maximum at φ=270°, i.e., 70° later than the maximum of flow rate. A similar delay has been observed in LES computations for the same combustor by Franzelli et al. [17] and Lourier et al. [18]. The mechanism that causes the delay between VF and ERF is revealed by phase-dependent fields of axial velocity and fuel distribution within the burner nozzle provided in Refs. [17, 18]: the axial velocity in the nozzle strongly oscillates by about ±150% around the mean value. The velocity within the fuel channels that inject fuel into the swirler, by contrast, remains relatively constant due to the larger pressure drop in the thin channels. Thereby a zone of fuel-rich gas accumulates during phases of low velocity in the swirler. This zone transported into the combustion chamber when the velocity in the nozzle increases. The

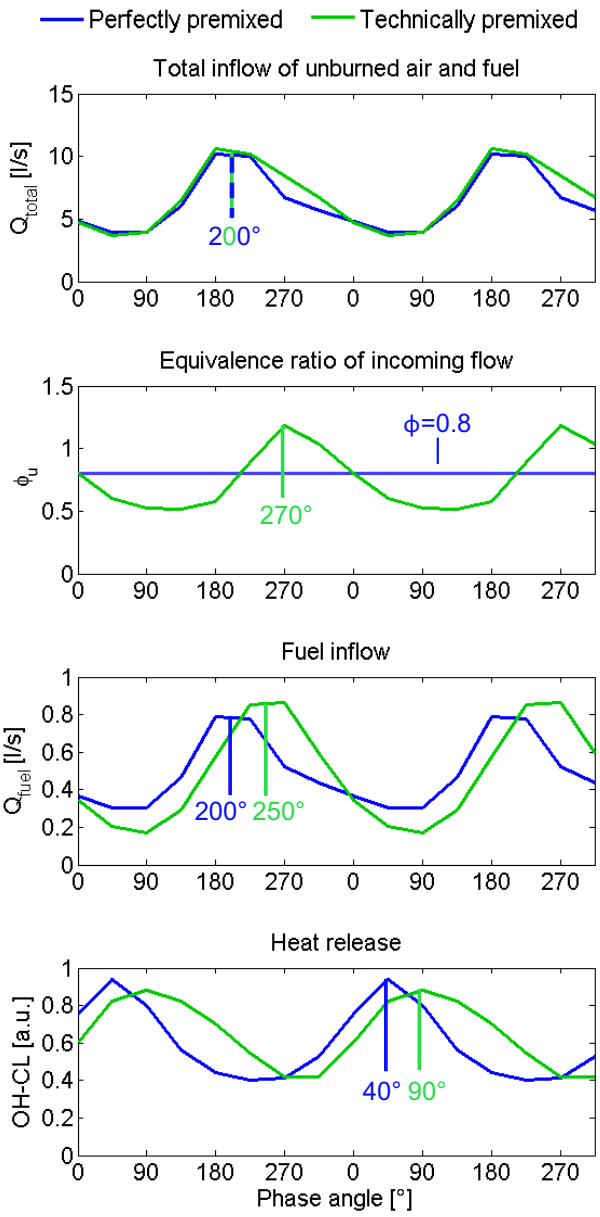

Figure 4: Phase-dependent oscillations of Q_{total}, ϕ_u, Q_{fuel} and heat release.

delay of the ERF therefore corresponds approximately to the convective transport time between the point of fuel injection in the swirler and the nozzle exit.

For the TP flame, the delay of ϕ_u with respect to Q_{total} causes a delay of the flow of unburned fuel into the chamber Q_{fuel}, which has its maximum at φ=250°. For the PP case with constant ϕ_u, by contrast, Q_{fuel} varies in the same way as Q_{total} with the maximum at φ=200°. After a certain delay for transport and mixing, the flames respond to an increase of Q_{fuel} with an increase of heat release. The respective heat release maxima at φ=40° and φ=90° show that this delay is 200° for both flames.

In conclusion, the feedback loop of the TP flame includes an additional convective delay time of 50° that is not present in PP mode. This time lag first delays Q_{fuel} and then heat release. The effect that heat release in a TP flame is delayed compared to the PP mode has been similarly found in an LES of another combustor [5]. For the frequency of 255 Hz of the TP flame, 50 ° corresponds to 0.5 ms. As specified in Table 1, the frequency of the TP flame is decreased compared to the PP case such that its oscillation period is increased by the same value, namely 3.9 ms−3.4 ms=0.5 ms. Therefore, the additional convective delay provides a reasonable explanation for the observed frequency decrease of the TP flame.

5. Transient interactions of VF and ERF

After the analysis of the global feedback cycle above, now the transient local mechanisms causing the distinctive dynamics of the TP flame presented in Sect. 4.1 will be discussed. Figure 5 shows an exemplary time-series of simultaneous stereo-PIV, OH-PLIF and acetone-PLIF measurements that cover one period of the acoustic cycle.

At t=0 ms (φ=5°), a zone of relatively fuel-rich unburned gas is seen in the range y<20 mm. This gas has entered through the nozzle during the previous maximum of ϕ_u at φ=270° (cf. Fig. 4) and was then convected into the chamber. At the inner border of the fuel-rich gas, intense reaction takes place as indicated by the high levels of OH. Due to the low axial velocity and the high flame speed of the fuel-rich gas, the reaction zone propagates radially outward into the stream of unburned gas. This further widens the flame base and narrows the stream of unburned gas as seen at t=0.4 and 0.9 ms.

During the time from 0.4 ms to 1.4 ms, the equivalence ratio of the incoming flow decreases, and consequently, the reaction at the flame base declines. At the same time, starting from t=0.9 ms, the velocity of the incoming flow increases signicantly until it reaches a maximum at t=1.9 ms. At t=1.9 ms, a region with virtually zero OH level appears in the inner shear layer above the nozzle, which indicates local flame extinction. Apparently this extinction is caused by flame stretch due to the combination of low equivalence ratio ($\phi_u \approx 0.6$ at φ=180°, cf. Fig. 4) and high velocity gradient [21, 22]. Narrowing and weaking of the flame root due to a decrease of equivalence ratio has also been reported for an inverse conical flame in a transverse acoustic field [23].

The low heat release and thus low thermal expansion together with the high inflow velocity induce a narrowed flame base and widened stream of unburned gas at t=2.4 ms. From t=1.4 ms until t=2.8 ms, the equivalence ratio and thereby also the flame speed of the incoming flow increases. This causes a re-ignition at the flame base at t=2.8 and 3.4 ms, and then a similar dynamics as described above starts over (not shown).

The OH-PLIF image series in Fig. 5 also reveals changes of flame surface density (FSD), which are another important part of flame response to ERF besides changes of flame speed and heating value [11]. It is seen that the lean reaction zones at t=1.4, 1.9 and 2.4 ms (indicated by low levels of OH) are mostly smooth and linear, whereas the fuel-rich reaction zones at t=3.4, 0 and 0.4 ms (indicated by high levels of OH) are often wrinkled and distorted. The according changes of FSD apparently conform with the varying heat release distributions

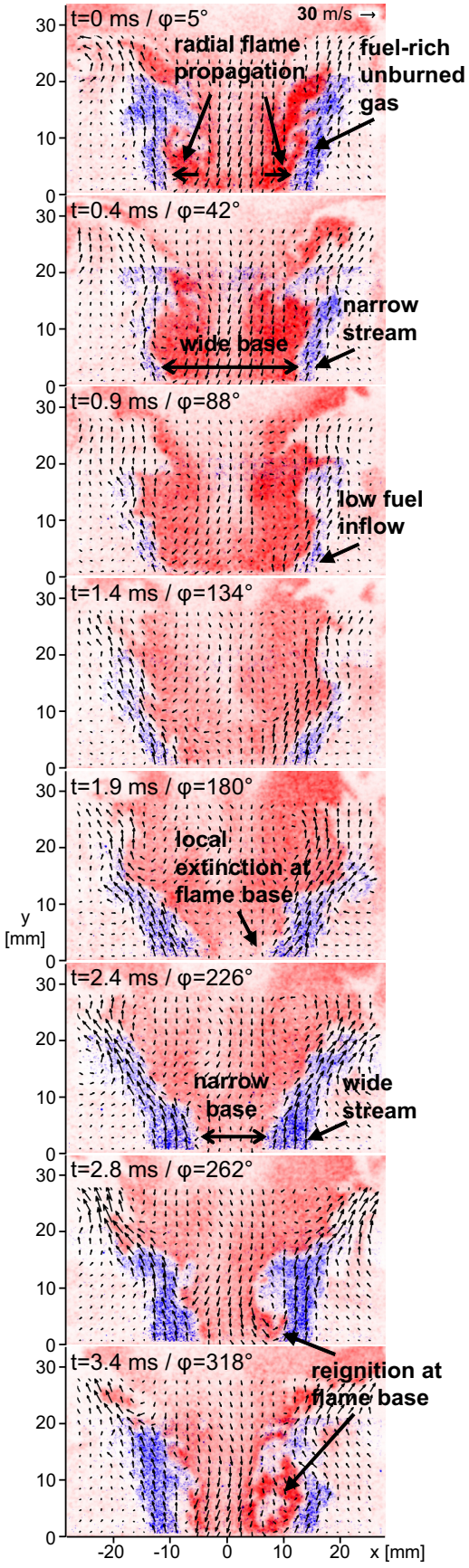

Figure 5: Time-series of simultaneous stereo-PIV (vectors), OH-PLIF (red) and acetone-PLIF (blue). The acetone-PLIF domain is limited to y<21 mm.

of the TP flame shown in Fig. 3, and thus show that variations of FSD are an important effect of ERF.

Taken together, the time-resolved measurements show that the changes of phase-dependent TP flame shape discussed in Sect. 4.1, namely widening/narrowing of flame base, partial extinction, and convective displacememt of heat release, all originate from transient interactions of VF and ERF. The phenomena further show that the time delay between VF and ERF is the essential parameter of this interaction: E.g., the partial extinction at φ=180° occurs because the increase of equivalence ratio is delayed to the velocity increase, and only thereby the combination of high velocity and low equivalence ratio that causes extinction can arise.

6. Summary and conclusions

The effects of equivalence ratio fluctuations (ERF) and their interaction with velocity fluctuations (VF) during thermoacoustic flame oscillations were studied experimentally in a gas turbine model combustor. In order to separate the effects of VF and ERF, the combustor has been operated in two configurations: a technically (i.e. partially) premixed (TP) configuration where both ERF and VF occur, and a perfectly premixed (PP) configuration where only VF are present. A particular operating condition was selected where the VF for both configurations are similar. In order to reveal the unsteady interactions of VF and ERF, time-resolved simultaneous measurements of flow field, flame structure and fuel distribution were performed using combined stereo-PIV, OH-PLIF and tracer-PLIF at a rate of 10 kHz.

In the first part of the analysis, phase-averaged velocity field, heat release and fuel distribution of the two modes were compared. Whereas the VF are almost identical, the corresponding fluctuations of heat release exhibit considerably different spatial patterns. In particular, periodic widening and narrowing as well as extinction and re-ignition of the flame base, and a convective displacement of the flame zone were observed in the TP flame but not in the PP case. An evaluation of the periodic variations of flux rates, ϕ and heat release further revealed that the feedback loop of the TP flame includes an additional convective delay time of 50°. This provided a reasonable explanation for the observed difference of oscillation frequency of the PP and TP flames.

In the second part, transient interactions of VF and ERF in the TP flame were studied using the time-resolved diagnostics. They showed that the specific changes of the TP flame shape seen in the phase-averaged analysis can be well explained by combined actions of VF and ERF. The observed extinction of the flame base, e.g., only can arise due to a coincidence of high velocity and low equivalence ratio. The results thereby demonstrate that the time delay between VF and ERF is the essential parameter of their interaction. The strong interplay of flow, mixing and reaction seen in the time-resolved measurements suggests that the effects of unsteady interactions of VF and ERF must be included in accurate predictive thermoacoustic models.

References

[1] T. Lieuwen, V. Yang, Combustion instabilities in gas turbine engines, Progress in Astronautics and Aeronautics, Vol. 210, AIAA, Washington, DC, 2005.

[2] D. Ducruix, T. Schuller, D. Durox, S. Candel, J. Propul. Power 19 (2003) 722-734.

[3] B. Schuermans, F. Guethe, D. Pennell, D. Guyot, C. O. Paschereit, J. Eng. Gas Turb. Power 132 (2010) 111503.

[4] K. T. Kim, J. G. Lee, B. D. Quay, D.A. Santavicca, Combust. Flame 157 (2010) 1731-1744.

[5] S. Hermeth, G. Staffelbach, L. Y. M. Gicquel, T. Poinsot, Proc. Combust. Inst. 34 (2013) 3165-3173.

[6] B. Čosič, S. Terhaar, J. P. Moeck, C. O. Paschereit, Combust. Flame 162 (2015) 1046-1062.

[7] B. Schuermans, V. Bellucci, F. Guethe, F. Meili, P. Flohr, Proc. ASME Turbo Expo (2004) GT2004-53831.

[8] T. Lieuwen, B. T. Zinn, Proc. Combust. Inst. 27 (1998) 1809-1816.

[9] J. G. Lee, K. Kim, D. A. Santavicca, Proc. Combust. Inst. 28 (2000) 415-421.

[10] T. Sattelmayer, J. Eng. Gas Turb. Power 125 (2003) 11–19.

[11] Shreekrishna, S. Hemchandra, T. Lieuwen, Combust. Theory Model. 14 (2010) 681–714.

[12] W. Meier, P. Weigand, X.R. Duan, R. Giezendanner-Thoben, Combust. Flame 150 (2007) 2-26.

[13] A. M. Steinberg, C. M. Arndt, W. Meier, Proc. Combust. Inst. 34 (2013) 3117-3125.

[14] K. Oberleithner, M. Stöhr, S. H. Im, C. M. Arndt, A. M. Steinberg, Combust. Flame 162 (2015) 3100-3114.

[15] C. Dem, M. Stöhr, C. M. Arndt, A. M. Steinberg, W. Meier, Z. Phys. Chem. 229 (2015) 569-595.

[16] S. Roux, G. Lartigue, T. Poinsot, U. Meier, C. Bérat, Combust. Flame 141 (2005) 40-54.

[17] B. Franzelli, E. Riber, L. Y. M. Gicquel, T. Poinsot, Combust. Flame 159 (2012) 621-637.

[18] J.-M. Lourier, B. Noll, M. Aigner, Proc. ASME Turbo Expo (2014) GT2014-26200.

[19] M. C. Thurber, F. Grisch, B. J. Kirby, M. Votsmeier, R. K. Hanson, Appl. Optics 37 (1998) 4963–4978.

[20] M. Stöhr, C. Arndt, W. Meier, Proc. Combust. Inst. 35 (2015) 3327-3335.

[21] Y. Ju, H. Guo, K. Maruta, F. Liu, J. Fluid Mech. 342 (1997) 315-334.

[22] M. Stöhr, C. Arndt, W. Meier, Proc. Combust. Inst. 34 (2013) 3107-3115.

[23] F. Baillot, F. Lespinasse, Combust. Flame 161 (2014) 1247-1267.